Jørgensen, B.B., D'Hondt, S.L., and Miller, D.J. (Eds.)
Proceedings of the Ocean Drilling Program, Scientific Results Volume 201

17. Data Report: Preservation of Bacterial Magnetosomes at Sites 1225 and 1227[1]

K.H. Ford,[2] J.W. King,[2] and S. Niitsuma[3]

ABSTRACT

Samples were collected at Sites 1225 and 1227 to investigate the occurrence of fine-grained, biogenic magnetic particles (magnetosomes). Several magnetic methods, including anhysteretic remanent magnetization and isothermal remanent magnetization, were used to characterize the main magnetic carriers in the samples. Extracts were made to isolate the fine-grained fraction, which was then examined under a transmission electron microscope. Grains with the unique characteristics of magnetosomes were found in samples from regions in the core with both high and low concentrations of magnetic minerals. This suggests they have the potential to be a persistent proxy of paleoredox conditions.

INTRODUCTION

Magnetotactic bacteria actively form intracellular chains of symmetrical, single-domain (40–100 nm) magnetic inclusions (magnetosomes) of magnetite, greigite, or pyrite (Frankel et al. 1983; Mann et al. 1990). These bacteria are microaerophilic, though they have been found in anoxic environments, both in the water column and at the surface/water interface (Stolz et al., 1990). It is presumed the magnetosomes serve to orient the bacterium vertically along lines of inclination (Frankel, 1984). It has been hypothesized that the composition and morphology of magnetosomes are associated with different environments of magnetic mineral formation and preservation (Hesse and Stolz, 1999). To

[1] Ford, K.H., King, J.W., and Niitsuma, S., 2006. Data report: Preservation of bacterial magnetosomes at Sites 1225 and 1227. *In* Jørgensen, B.B., D'Hondt, S.L., and Miller, D.J. (Eds.), *Proc. ODP, Sci. Results,* 201, 1–17 [Online]. Available from World Wide Web: <http://www-odp.tamu.edu/publications/201_SR/VOLUME/CHAPTERS/115.PDF>. [Cited YYYY-MM-DD]
[2] University of Rhode Island, Graduate School of Oceanography, Narragansett RI, 02882, USA.
kathryn.ford@state.ma.us
[3] Graduate School of Science, Tohoku University, Sendai 980-8578, Japan.

Initial receipt: 26 July 2004
Acceptance: 1 February 2006
Web publication: 12 June 2006
Ms 201SR-115

the extent that this hypothesis is true, the magnetic mineral composition and morphology may be used to fingerprint paleoredox conditions and specific biological activities throughout Earth history. As potential sedimentary recorders of changing geochemical environments, bacterial magnetosomes may also persist longer than other proxies.

In order to investigate the relationship between magnetosomes and the redox environment, the magnetic components of samples from Holes 1225A, 1225C, and 1227B were examined. These samples represent two different sedimentary and reduction-diagenesis regimes. Site 1225 has pore water sulfate throughout the sediment column, no sulfide, a significant dissolved iron and magnetic susceptibility correlation, and electron acceptors at the bottom of sediment column. Site 1227 is organic rich and has a clear reduction-diagenesis sequence in the uppermost 20 m, with a sulfate–sulfide transition and low pore water iron concentrations.

PROCEDURE/METHODS

Sample Selection and Storage

Shipboard records of magnetic susceptibility (K) from whole cores run on the multisensor track were used to select sections with higher susceptibility (5×10^{-5} to 10×10^{-5} SI units) for sampling. The regions focused on were 0–70 meters below seafloor (mbsf) at Site 1225, 200–250 mbsf at Site 1225, and 0–20 mbsf at Site 1227. Some samples from sections with low susceptibility (~0), such as 80–200 mbsf at Site 1225 and below 20 mbsf at Site 1227, were selected for comparison. Samples were taken using plastic, 10-cm^3 round samplers and stored anaerobically in sealed foil bags with an oxygen scrubber. They were kept refrigerated until sampling, at which point they were warmed to room temperature. Following sampling, the remainder of each sample was stored refrigerated in a sealed plastic bag.

Bulk Magnetic Measurements

The single samples were measured for magnetic susceptibility, including frequency-dependent magnetic susceptibility. Samples were measured in a 0.1-mT induction at low frequency (K_{LF}) and at high frequency (K_{HF}). The results were corrected for volume. Frequency-dependent susceptibility for those samples measured at both high and low frequency was expressed as K_{LF}:K_{HF}.

The bulk sediment was further characterized by measuring anhysteretic remanent magnetization (ARM) on a 2G Enterprises cryogenic magnetometer. The peak alternating field was 0.1 T, and the steady field was 0.1 mT. The samples were normalized to the steady field and expressed as K_{ARM}. Saturation isothermal remanent magnetization (SIRM) was induced with an electromagnet at 1.3 T and measured on the magnetometer. An induced back–isothermal remanent magnetism (IRM) was imparted by subjecting the samples to a reversed field of 0.3 T. The S-ratio, a measure of the proportion of higher coercivity magnetic minerals to lower coercivity magnetic minerals, was calculated using the following formula:

$$-\mathrm{IRM}_{-0.3\mathrm{T}}/\mathrm{SIRM}. \quad (1)$$

The hysteresis parameters of a dried subsample with a mass of ~0.01 g were measured on a Princeton Measurements Corporation Micromag 2900 alternating gradient force magnetometer.

Magnetic Extractions

Both fine-grained (<7 µm) and coarse-grained (>7 µm) material were extracted for microscopic study. The residues following the extractions were compared to bulk measurements to examine extraction efficiency. The following procedure, adopted from Peck and King (1996), was used:

1. A total of 4 cm^3 of sediment per sample was disaggregated with deionized water (DI) into slurry, preserved with 5 mL of formalin, and wet-sieved using a 7-µm sieve.
2. The <7-µm sediment slurry fraction was dispersed in 400 mL of DI and circulated for 80 hr past a magnetized needle enclosed in a latex sleeve (Fig. F1). The slurry was passed through a closed and dust-free circulation system (using a peristaltic pump). During circulation, the needle was removed once every 20 hr. The attached magnetic grains were collected by removing the sleeve and rinsing into a Petri dish. This <7-µm extract was further refined by concentration with a handheld Nd supermagnet held under the dish then pipetted onto a carbon-coated copper grid and analyzed on a JEOL 1200 EX transmission electron microscope (TEM).
3. After 80 hr, the remaining slurry was removed from the circulation system, dried at 45°C, and measured for hysteresis parameters on the Micromag 2900.
4. The magnetic component of the >7-µm sediment slurry fraction was dispersed in 150 mL of DI and extracted by agitating with a Nd-Fe-B supermagnet enclosed in a brass housing. The extract was then rinsed into a new container and the process was repeated until no particles were visible on the brass housing. This extract was concentrated using a handheld supermagnet held on the outside wall of the container and pipetted onto a carbon-coated copper grid and analyzed on a JEOL 1200 EX TEM.
5. The postextraction residue from the >7-µm sediment slurry was dried at 45°C and measured for hysteresis parameters on a Micromag 2900.

RESULTS

Selection of Samples for Extraction

Because of the time-consuming nature of the extraction procedure, samples were selected discriminately to represent areas where the bulk magnetic properties were suggestive of fine-grained magnetic minerals, with a few samples also being extracted from low-susceptibility regions for comparison. Fine-grained magnetic minerals are characterized by high K_{ARM}/K. In order to exclude super-paramagnetic particles, which could dominate the K_{ARM}/K measurements, the frequency dependence of the susceptibility was also measured on the single samples (Figs. F2, F3). Data are provided in Tables T1 and T2.

F1. Magnetized needle, p. 7.

F2. Magnetic susceptibility, Holes 1225A and 1225C, p. 8.

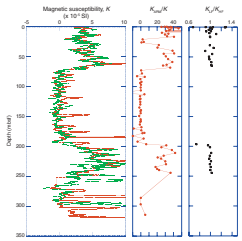

F3. Magnetic susceptibility, Holes 1227A and 1227D, p. 9.

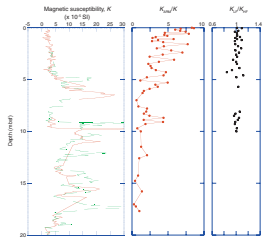

T1. Susceptibility and ARM data, Site 1225, p. 15.

T2. Susceptibility and ARM data, Site 1227, p. 16.

Extraction of Fine Grains

The grains that were extracted and viewed with the TEM fit the characteristics of magnetosomes: they ranged from 40 to 100 nm, occurred in chains, and had symmetrical shapes (Fig. F4). The entire image collection is available through the ODP Data Librarian. The grains were found in a variety of morphotypes (even within a single chain) and without membranes; therefore, they are most likely fossils rather than from living bacteria.

In order to ascertain the efficiency of the extraction, the bulk sample hysteresis properties were compared to the residue following extraction. The shift to larger grain sizes, from pseudosingle domain to multidomain, following the removal of the <7-µm fraction suggests significant removal of fine-grained magnetic particles (Fig. F5). Saturation magnetization (*Ms*) was used to calculate the extraction efficiency with the following formula:

$$[(Ms_{bulk} - Ms_{residue})/Ms_{bulk}] \times 100. \quad (2)$$

Efficiency ranged from 10% to 98%. Samples with poor extraction efficiency typically had low *Ms*. Because the extraction method is biased toward minerals with high *Ms* (Peck and King, 1996), this was expected.

Mineralogy

In order to determine the main magnetic carrier in the bulk samples, the S-ratio was calculated by comparing IRM to back-IRM. Back-IRM was ~1, which is indicative of magnetite at Site 1225 (Table T3). Additionally, the extent of oxidation was examined by remeasuring the ARM of the original samples following 2 yr of refrigeration (41°C) while being kept wet but exposed to air (Fig. F6). The decrease in ARM could be an indicator of greigite because it is more susceptible to oxidation than other magnetic carriers (Snowball and Thompson, 1990). **Niitsuma et al.** (this volume) used the Verwey transition to identify magnetite as the main magnetic carrier at Site 1225. Shipboard X-ray diffraction of extracts from 5, 10, and 47 mbsf at Site 1227 suggest magnetite is the main magnetic carrier at that site (D'Hondt, Jørgensen, Miller, et al., 2003). Although there is definitive evidence of magnetite present in the samples, the presence or absence of greigite was not conclusive.

Comparison to Other Parameters

Interestingly, we did find magnetosomes in the low-susceptibility region between 70 and 200 mbsf at Site 1225 (Fig. F7). Similarly, at Site 1227, there was preservation even as sulfide was increasing (Fig. F8). With further examination of the mineralogy of the individual grains and the abundance of the magnetosomes, a better understanding of the preservation potential of magnetosomes and their links to redox conditions will be possible.

ACKNOWLEDGMENTS

The authors would like to thank Ben Swanson, Andrea Mullen, and Chip Heil for helping with laboratory work. Paul Johnson provided as-

F4. TEM images of magnetosomes, p. 10.

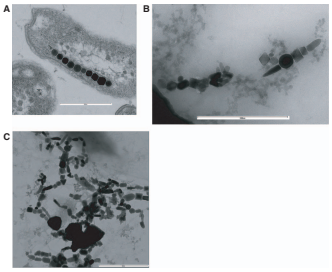

F5. *Mr*/*Ms* plots, p. 11.

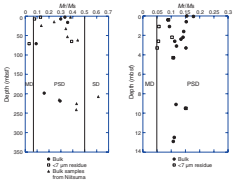

T3. S-ratio, Site 1225, p. 17.

F6. ARM measurements, Sites 1225 and 1227, p. 12.

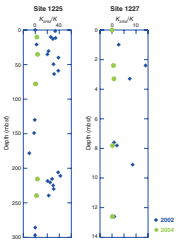

F7. Site 1225, p. 13.

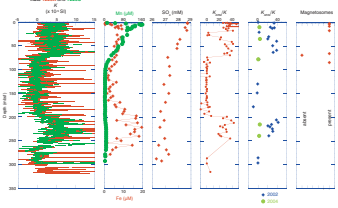

F8. Site 1227, p. 14.

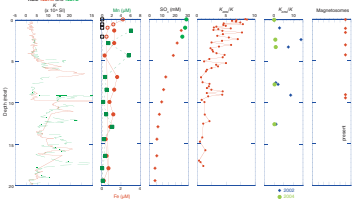

sistance with TEM imaging, and many thanks to Steve D'Hondt and other Leg 201 scientists for thoughtful conversations. This manuscript was improved by the helpful revisions of Robert Musgrave. This research used samples and/or data provided by the Ocean Drilling Program (ODP). ODP is sponsored by the U.S. National Science Foundation (NSF) and participating countries under management of Joint Oceanographic Institutions (JOI), Inc. Funding for this research was provided by U.S. Science Advisory Committee (USSAC).

REFERENCES

Frankel, R.B., 1984. Magnetic guidance of microorganisms. *Annu. Rev. Biophys. Biophys. Chem.,* 13:85–103. **doi:10.1146/annurev.bb.13.060184.000505**

Frankel, R.B., Papaefthymiou, G.C., Blakemore, R.P., and O'Brien, W., 1983. Fe_3O_4 precipitation in magnetotactic bacteria. *Geochim. Cosmochim. Acta.,* 763:147–159.

Hesse, P.P., and Stolz, J.F., 1999. Bacterial magnetite and the Quaternary climate record. *In* Maher, B.A., and Thompson, R. (Eds.), *Quaternary Climates, Environments, and Magnetism:* Cambridge (Cambridge Univ. Press), 163–198.

Mann, S., Sparks, N.H.C., Frankel, R.B., Bazylinski, D.A., and Jannasch, H.W., 1990. Biomineralization of ferrimagnetic greigite (Fe_3S_4) and iron pyrite (FeS_2) in a magnetotactic bacterium. *Nature (London, U. K.),* 343:258–261. **doi:10.1038/343258a0**

Peck, J.A., and King, J.W., 1996. Magnetofossils in the sediment of Lake Baikal, Siberia. *Earth Planet. Sci. Lett.,* 140:159–172. **doi:10.1016/0012-821x(96)00027-1**

Snowball, I., and Thompson, R., 1990. A stable chemical remanence in Holocene sediments. *J. Geophys. Res.,* 95:4471–4479.

Stolz, J.F., Lovley, D.R., and Haggerty, S.E., 1990. Biogenic magnetite and the magnetization of sediments. *J. Geophys. Res.,* 95:4355–4361.

Figure F1. Magnetized needle used for extraction of <7-µm size fraction. Coin diameter = 24 mm.

Figure F2. Hole 1225A (red) and 1225C (green) shipboard magnetic susceptibility, smoothed using a 2-m moving average. Also shown are single sample magnetic susceptibility/magnetic susceptibility normalized to the steady field (K_{ARM}/K) and frequency-dependent susceptibility. K_{LF} = low frequency, K_{HF} = high frequency.

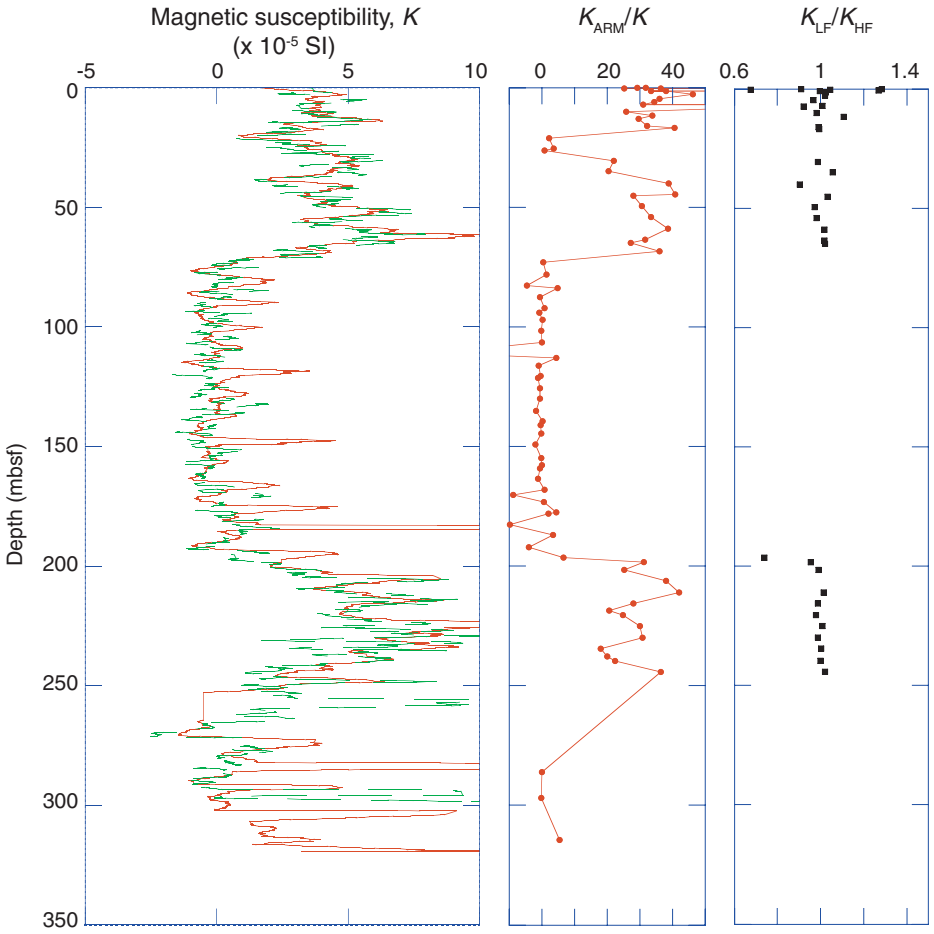

Figure F3. Hole 1227A (red) and 1227D (green) shipboard magnetic susceptibility, smoothed using a 2-m moving average. Also shown are single sample magnetic susceptibility/magnetic susceptibility normalized to the steady field (K_{ARM}/K) and frequency-dependent susceptibility. K_{LF} = low frequency, K_{HF} = high frequency.

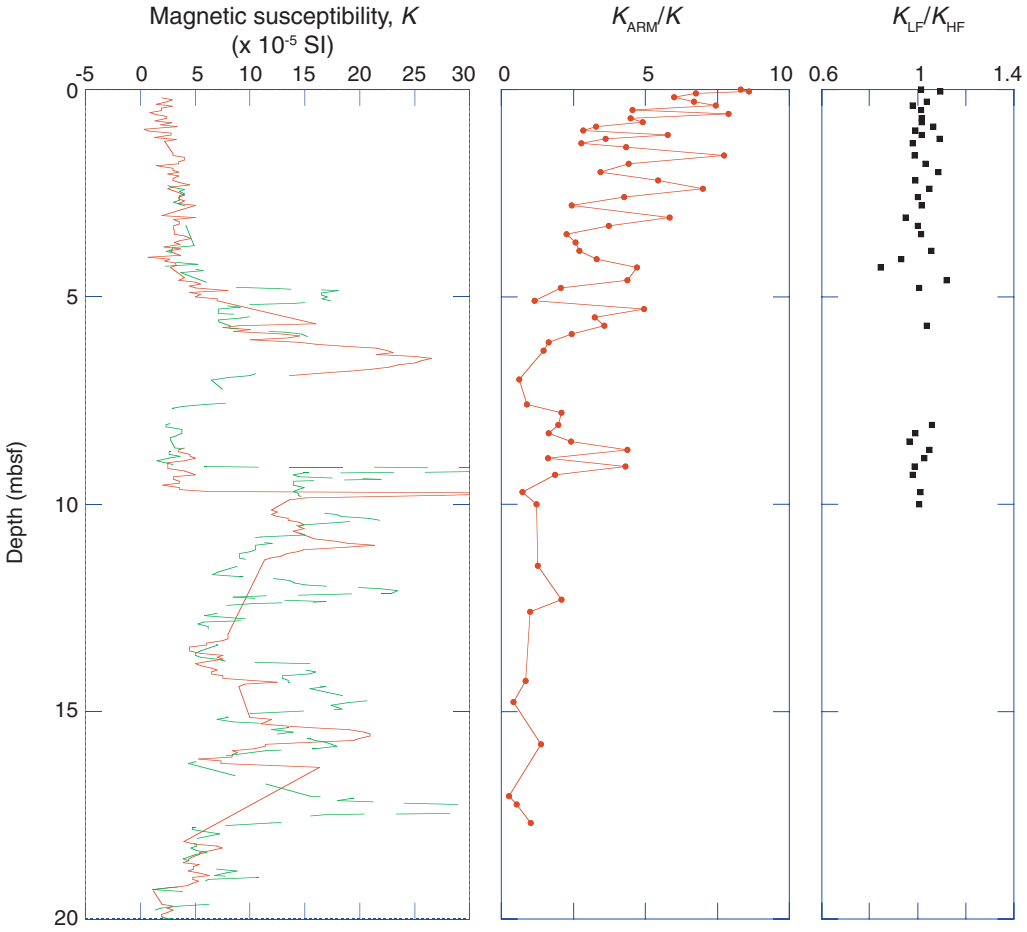

Figure F4. TEM images of magnetosomes. **A.** From a living magnetotactic bacterium from Pettaquamscutt River, Rhode Island (courtesy of Paul Johnson, University of Rhode Island). **B.** From Section 201-1225C-1H-5; 7.48 mbsf. **C.** From Section 201-1227B-1H-2; 1.6 mbsf.

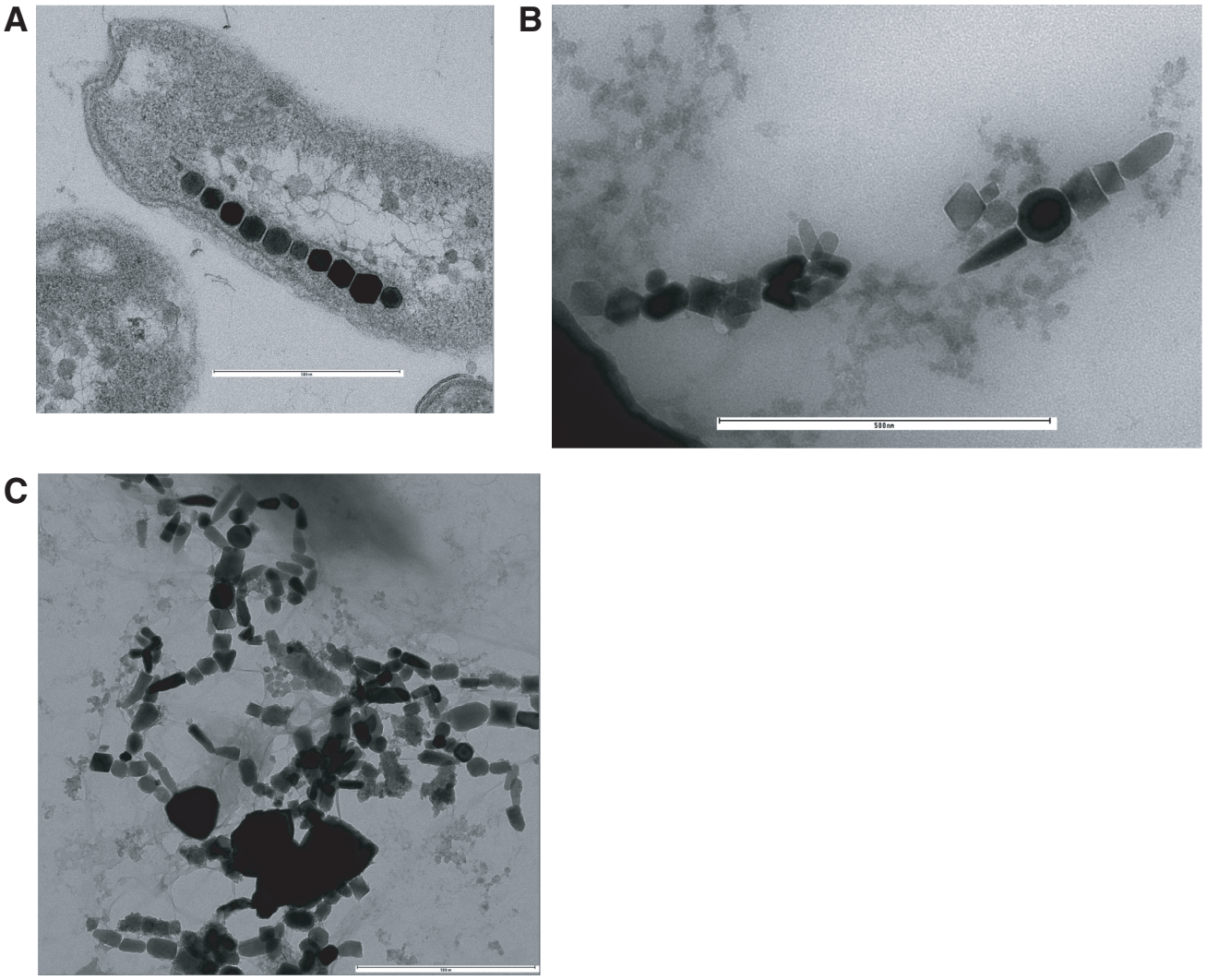

Figure F5. *Mr*/*Ms* plots. In bulk samples, including samples processed by **Niitsuma et al.** (this volume), compared to samples with grains <7 µm removed. MD = multidomain, PSD = pseudosingle domain, SD = single domain.

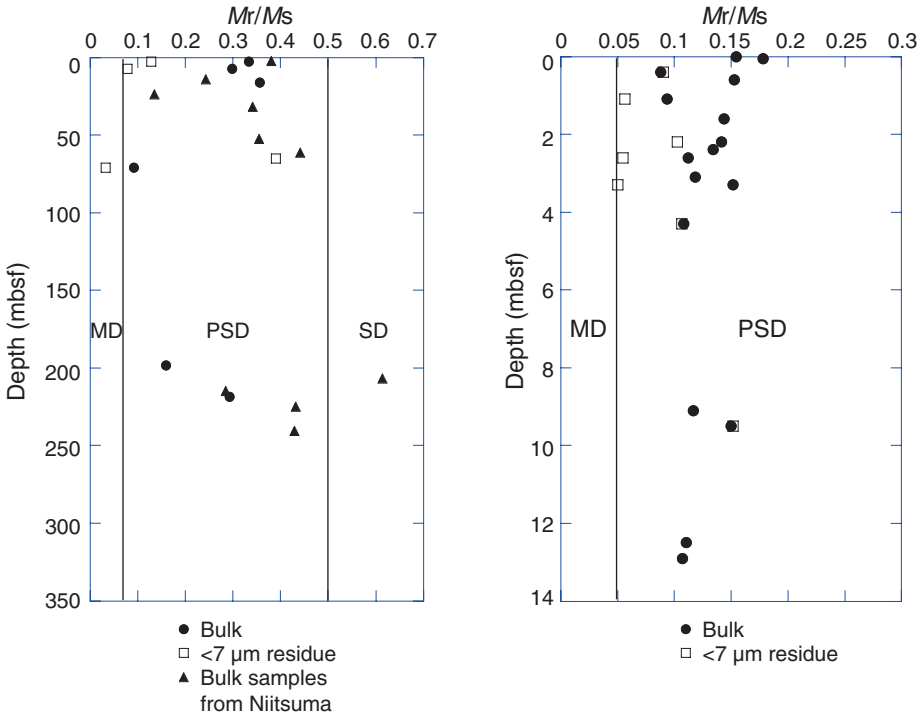

Figure F6. ARM measurements from Sites 1225 and 1227 compared between 2002 and 2004. K = magnetic susceptibility, K_{ARM} = magnetic susceptibility normalized to the steady field.

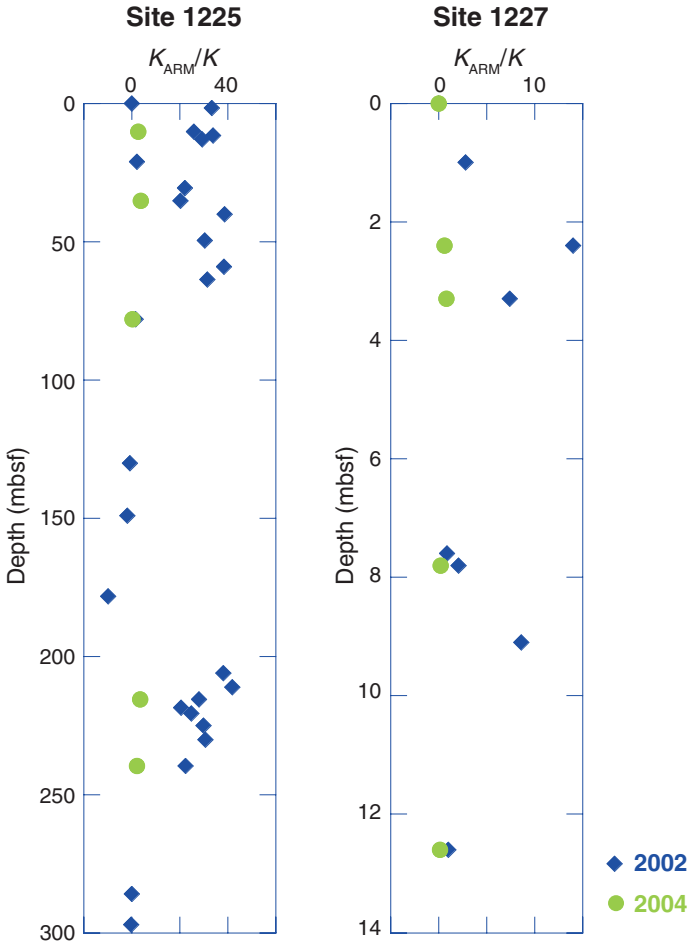

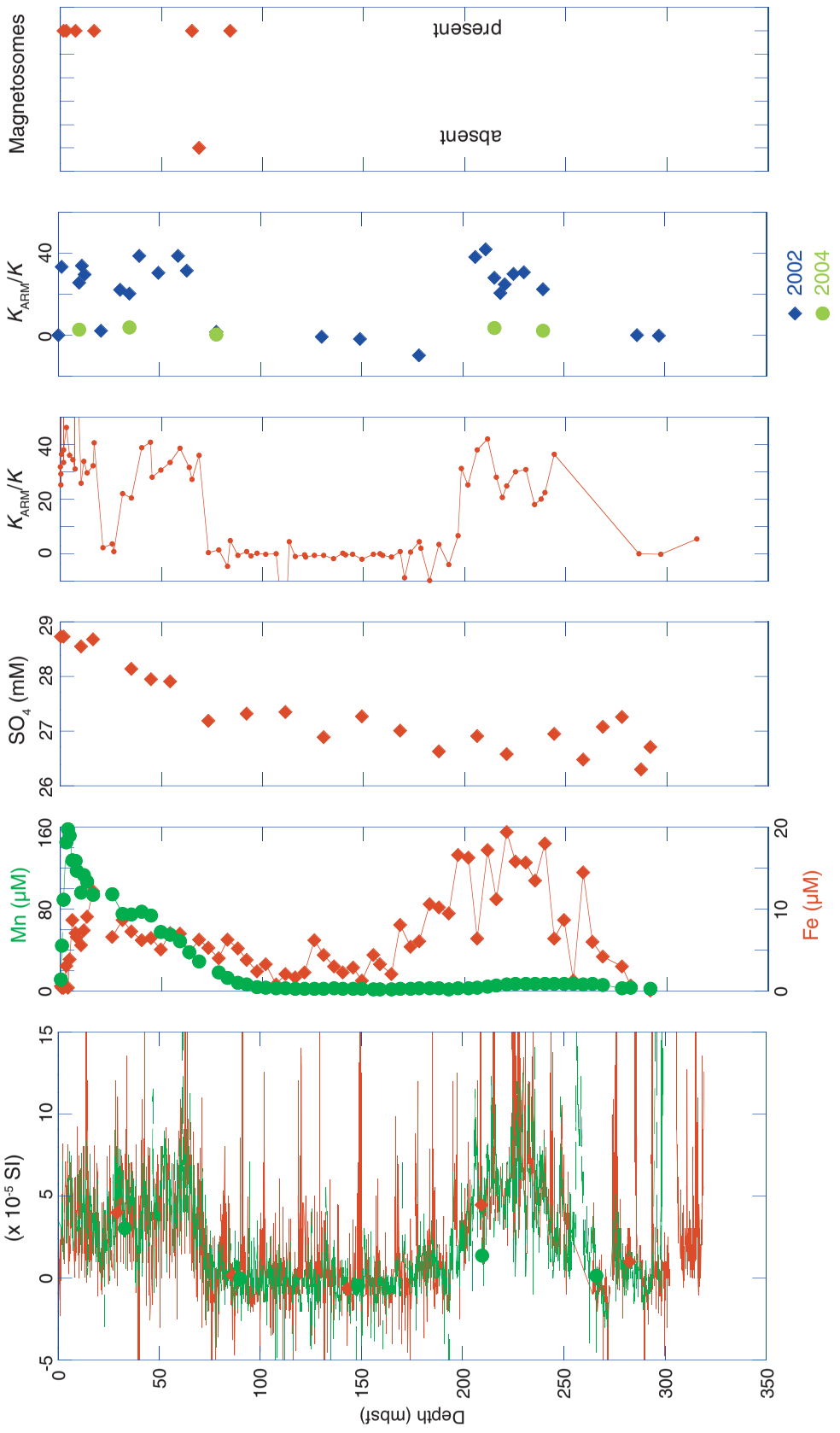

Figure F7. Site 1225. K = magnetic susceptibility, K_{ARM} = magnetic susceptibility normalized to the steady field.

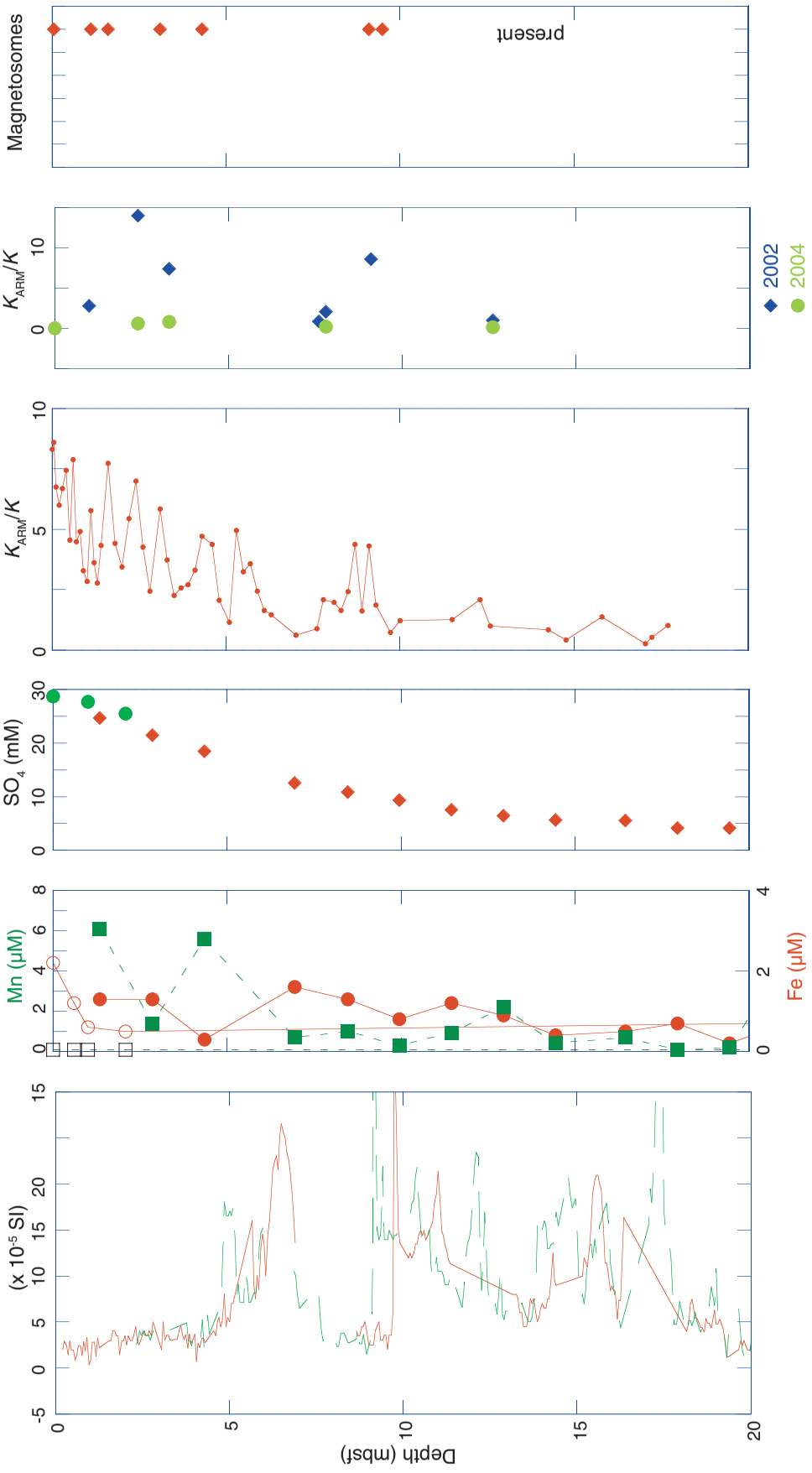

Figure F8. Site 1227. K = magnetic susceptibility, K_{ARM} = magnetic susceptibility normalized to the steady field.

Table T1. Susceptibility and ARM data, Site 1225.

Hole, core, section, interval (cm)	Depth (mbsf)	K ($\times 10^{-5}$ SI)	K_{ARM} ($\times 10^{-4}$ SI)	K_{ARM}/K
201-				
1225B-1H-1, 0	0	0.895	2.85	31.87
1225B-1H-1, 21	0.21	1.85	5.42	29.30
1225C-1H-1, 35	0.35	2.454	6.21	25.32
1225B-1H-1, 42	0.42	1.432	5.24	36.57
1225B-1H-1, 62	0.62	0.716	4.31	60.18
1225B-1H-1, 80	0.8	0.656	3.92	59.82
1225B-1H-1, 101	1.01	0.239	2.99	124.95
1225C-1H-2, 15	1.65	3.651	12.24	33.53
1225A-1H-2, 15	1.65	3.126	11.93	38.16
1225C-1H-2, 148	2.98	2.334	10.82	46.35
1225C-1H-4, 15	4.65	3.651	13.21	36.17
1225C-1H-5, 15	6.15	2.394	8.24	34.42
1225A-2H-2, 148	7.28	2.405	7.49	31.16
1225C-1H-5, 148	7.48	0.539	4.05	75.13
1225C-2H-2, 0	10.3	2.215	5.73	25.88
1225C-2H-2, 133	11.63	0.599	2.03	33.95
1225C-2H-3, 133	13.13	1.556	4.61	29.62
1225C-2H-5, 133	16.13	3.094	9.95	32.16
1225A-3H-3, 0	16.8	2.104	8.54	40.59
1225C-3H-2, 133	21.13	0.658	0.15	2.27
1225C-3H-5, 133	25.63	0.239	0.09	3.66
1225A-4H-2, 148	26.28	0.962	0.09	0.89
1225C-4H-2, 133	30.63	4.01	8.88	22.14
1225C-4H-5-133	35.13	2.514	5.12	20.37
1225C-5H-2, 133	40.13	1.077	4.19	38.88
1225C-5H-5, 133	44.63	1.796	7.33	40.80
1225A-6H-2, 148	45.28	2.405	6.75	28.07
1225C-6H-2, 131	49.61	3.292	10.06	30.57
1225C-6H-5, 132	54.12	3.531	11.79	33.39
1225C-7H-2, 133	59.13	3.052	11.80	38.67
1225C-7H-5, 133	63.63	2.274	7.20	31.67
1225A-8H-3, 71	65.01	5.711	15.58	27.28
1225C-8H-2, 133	68.63	3.112	11.22	36.05
1225C-8H-5, 133	73.13	1.436	0.06	0.40
1225C-9H-2, 133	78.13	0.18	0.03	1.59
1225C-9H-5, 133	82.63	–0.06	0.03	–4.53
1225A-10H-3, 72	84.02	0.06	0.03	4.85
1225C-10H-2, 133	87.63	–0.06	0.00	–0.47
1225C-10H-5, 133	92.13	0.239	0.02	0.79
1225A-11H-3, 132	94.12	–0.18	0.01	–0.76
1225C-11H-2, 133	97.13	0.479	0.01	0.24
1225C-11H-5, 133	101.63	–0.359	0.01	–0.16
1225C-12H-2, 133	106.63	0	0.02	0.00
1225C-12H-5, 133	111.13	–0.12	0.35	–28.85
1225A-13H-3, 132	113.11	0.778	0.35	4.46
1225C-13H-2, 133	116.13	–0.181	0.02	–0.94
1225C-13H-5, 133	120.63	–0.239	0.01	–0.34
1225A-14H-2, 14	121.28	–0.181	0.02	–1.12
1225C-14H-2, 133	125.63	–0.421	0.03	–0.60
1225C-14H-5, 133	130.13	–0.301	0.02	–0.56
1225C-15H-2, 133	135.13	–0.119	0.02	–1.80
1225C-15H-5, 133	139.63	0.239	0.01	0.34
1225A-16H-3, 77	141.07	–0.421	0.02	–0.37
1225C-16H-2, 129	144.59	–0.542	0.00	–0.08
1225C-16H-5, 133	149.13	–0.06	0.01	–1.83
1225C-17H-3, 117	154.85	–0.301	0.00	–0.12
1225C-17H-5, 133	157.87	–0.119	0.00	0.00
1225A-18H-2, 148	159.28	–0.419	0.02	–0.51
1225C-18H-2, 133	163.63	–0.18	0.02	–1.06
1225C-18H-5, 133	168.13	0.537	0.04	0.78
1225A-19H-3, 133	170.13	–0.06	0.05	–8.62
1225C-19H-2, 133	173.13	0.301	0.02	0.65
1225C-19H-5, 133	177.48	0.776	0.35	4.47
1225A-20H-2, 148	178.28	0.239	0.05	1.98
1225C-20H-2, 133	182.63	–0.06	0.06	–9.79
1225C-20H-5, 133	187.13	0.18	0.06	3.36
1225C-21H-2, 133	192.13	–0.119	0.05	–3.84
1225C-21H-5, 133	196.63	0.119	0.08	6.60
1225A-22H-3, 105	198.35	0.658	2.06	31.38
1225C-22H-2, 133	201.63	1.804	4.54	25.14
1225C-22H-5, 133	206.13	3.667	14.00	38.17
1225C-23H-2, 133	211.13	2.529	10.64	42.06
1225C-23H-5, 134	215.64	2.508	7.06	28.15
1225A-24H-3, 84	218.64	3.974	8.25	20.75
1225C-24H-2, 133	220.63	3.643	9.10	24.98
1225C-24H-5, 133	225.13	3.853	11.59	30.08
1225C-25H-2, 133	230.13	4.569	14.10	30.86
1225C-25H-5, 133	234.63	5.147	9.29	18.06
1225A-26H-3, 89	237.69	4.094	8.20	20.02
1225C-26H-2, 133	239.63	6.141	13.84	22.54
1225C-26H-5, 133	244.13	2.269	8.28	36.50
1225A-32H-2, 148	286.05	1.676	0.02	0.10
1225A-33H-3, 131	297.01	–0.602	0.00	–0.02
1225A-35X-1, 143	314.63	1.257	0.69	5.51

Table T2. Susceptibility and ARM data, Site 1227.

Core, section, interval (cm)	Depth (mbsf)	K ($\times 10^{-5}$ SI)	K_{ARM} ($\times 10^{-4}$ SI)	K_{ARM}/K
201-1227B-				
1H-1, 0	0	1.14	9.48	8.32
1H-1, 5	0.05	1.38	11.86	8.60
1H-1, 10	0.1	1.32	8.91	6.75
1H-1, 2	0.2	1.62	9.73	6.01
1H-1, 30	0.3	2.219	14.82	6.68
1H-1, 40	0.4	1.44	10.73	7.45
1H-1, 50	0.5	1.92	8.75	4.56
1H-1, 60	0.6	0.9	7.09	7.88
1H-1, 70	0.7	1.56	7.01	4.49
1H-1, 80	0.8	1.08	5.30	4.91
1H-1-90	0.9	1.32	4.34	3.29
1H-1, 100	1	1.74	4.95	2.85
1H-1, 110	1.1	2.039	11.76	5.77
1H-1, 120	1.2	1.5	5.43	3.62
1H-1, 130	1.3	2.639	7.35	2.78
1H-1, 140	1.4	2.759	11.98	4.34
1H-2, 10	1.6	0.9	6.96	7.74
1H-2, 30	1.8	0.9	3.98	4.42
1H-2, 50	2	1.44	4.95	3.44
1H-2, 70	2.2	1.32	7.19	5.45
1H-2, 90	2.4	1.62	11.33	7.00
1H-2, 110	2.6	0.84	3.59	4.27
1H-2, 130	2.8	2.939	7.20	2.45
1H-3, 10	3.1	0.54	3.16	5.84
1H-3, 30	3.3	0.96	3.57	3.72
1H-3, 50	3.5	1.8	4.09	2.27
1H-3, 70	3.7	1.62	4.19	2.59
1H-3, 90	3.9	1.86	5.05	2.71
1H-3, 110	4.1	1.08	3.59	3.32
1H-3, 130	4.3	0.72	3.39	4.71
1H-4, 10	4.6	2.159	9.44	4.37
1H-4, 30	4.8	6.234	12.88	2.07
2H-1, 20	5.1	5.994	6.96	1.16
2H-1, 30	5.3	2.577	12.77	4.96
2H-1, 50	5.5	3.071	9.94	3.24
2H-1, 70	5.7	5.155	18.40	3.57
2H-1, 90	5.9	4.795	11.75	2.45
2H-1, 110	6.1	10.13	16.59	1.64
2H-1, 130	6.3	12.767	18.81	1.47
2H-2, 50	7	5.754	3.52	0.61
2H-2, 110	7.6	3.477	3.12	0.90
2H-2, 130	7.8	1.558	3.26	2.09
2H-3, 10	8.1	0.945	1.86	1.97
2H-3, 30	8.3	2.274	3.76	1.65
2H-3, 50	8.5	2.274	5.53	2.43
2H-3, 70	8.7	1.436	6.27	4.37
2H-3, 90	8.9	1.654	2.70	1.63
2H-3, 110	9.1	1.257	5.40	4.30
2H-3, 130	9.3	1.536	2.86	1.86
2H-4, 22	9.72	17.177	12.78	0.74
2H-4, 50	10	7.601	9.38	1.23
2H-5, 50	11.5	4.369	5.53	1.27
2H-5, 130	12.3	5.387	11.25	2.09
2H-6, 10	12.6	4.968	4.95	1.00
2H-7, 15	14.27	5.865	4.96	0.85
3H-1, 27	14.77	11.132	4.56	0.41
3H-1, 130	15.8	4.848	6.65	1.37
3H-2, 105	17.05	16.878	4.64	0.27
3H-2, 125	17.25	21.204	11.51	0.54
3H-3, 20	17.7	3.591	3.68	1.03

Table T3. Site 1225 S-ratio.

Hole, core, section, interval (cm)	Depth (mbsf)	Forward-IRM (mA/m)	Back-IRM (mA/m)	S-ratio
201-				
1225C-1H-2, 15	1.65	–1.45E–03	1.39E–03	0.96
1225C-2H-2, 0	10.3	–7.63E–04	7.39E–04	0.97
1225C-2H-2, 133	11.63	–7.27E–04	7.25E–04	1.00
1225C-2H-3, 133	13.13	–6.30E–04	6.14E–04	0.97
1225C-3H-2, 133	21.13	–9.91E–05	8.15E–05	0.82
1225C-4H-2, 133	30.63	–8.31E–05	6.94E–05	0.84
1225C-4H-5, 133	35.13	–1.15E–03	9.69E–04	0.85
1225C-5H-2, 133	40.13	–4.26E–04	4.56E–04	1.07
1225C-6H-2, 131	49.61	–8.86E–04	7.54E–04	0.85
1225C-7H-2, 133	59.13	–1.08E–03	1.03E–03	0.96
1225C-7H-5, 133	63.63	–1.46E–03	1.38E–03	0.95
1225C-9H-2, 133	78.13	–2.71E–05	2.23E–05	0.82
1225C-14H-5, 133	130.13	2.70E–05	–2.84E–05	1.05
1225C-16H-5, 133	149.13	–1.52E–05	1.54E–05	1.01
1225C-20H-2, 148	178.28	2.81E–05	–2.89E–05	1.03
1225C-22H-5, 133	206.13	–1.25E–03	1.31E–03	1.05
1225C-23H-2, 133	211.13	–1.10E–03	1.07E–03	0.97
1225C-23H-5, 134	215.64	–8.21E–04	7.61E–04	0.93
1225A-24H-3, 84	218.64	5.87E–04	–6.15E–04	1.05
1225C-24H-2, 133	220.63	9.63E–04	–9.02E–04	0.94
1225C-25H-2, 133	230.13	1.22E–03	–1.29E–03	1.06
1225C-26H-2, 133	239.63	1.57E–03	–1.65E–03	1.05
1225A-32H-2, 148	286.05	1.70E–04	–1.74E–04	1.02
1225A-33H-3, 131	297.01	1.29E–05	–1.26E–05	0.98